Supporting Information for

Highly Conductive $Cu_{2-x}S$ Nanoparticle Films through Room Temperature Processing, and an Order of Magnitude Enhancement of Conductivity via Electrophoretic Deposition

*Obafemi O. Otelaja, Don-Hyung Ha, Tiffany Ly, Haitao Zhang, and Richard D. Robinson**

**Corresponding author email: rdr82@cornell.edu*

Further Details on Experimental Methods

Chemicals: Hexanes (≥98.5%), ethanol (≥99.5%), ammonium sulfide (40-48 wt% solution in water), oleylamine (70%), copper(I) chloride (99.995%) were purchased from Aldrich. Molecular sieves (UOP type 3 Å) were also purchased from Aldrich and activated at 300 ^{o}C under dynamic vacuum for 3 hours before use.

***Synthesis*:** A large-scale synthesis of $Cu_{2-x}S$ nanoparticles followed standard procedures.[1] The synthesis was carried out in a dry, oxygen-free, dinitrogen atmosphere by employing standard Schlenk line and glove box techniques. A mixture of 1 g copper (I) chloride and 10 mL oleylamine was heated at 80 °C until the solution became clear. Temperature was then lowered to ~50 °C and 10 mL molecular sieve-dried $(NH_4)_2S$ oleylamine solution (0.5 mmol/mL) was added. The reaction was kept for 5 mins and the reaction flask was then immersed into an oil bath which has been pre-heated to 180 °C. The reaction was allowed to proceed for 40 mins and cooled down by removing oil bath. Ethanol was added to the solution to precipitate out nanoparticles, which were separated by centrifugation and washed one more time with hexanes/ethanol. The purified NCs were dissolved in hexanes. The prepared nanoparticles were stored in ambient conditions prior to utilization for transport studies. Although the particles have likely aged, all comparisons of EPD and spin-casting are for films made from the same stock of re-dispersed nanoparticles.

Transmission Electron Microscopy: TEM images of the nanoparticle samples were obtained using a FEI Tecnai F12 microscope operating at 120 keV. At least 100 particles were analyzed per sample to obtain a representative size distribution.

X-ray Diffraction: XRD (X-ray diffraction) spectra were collected using a Bruker General Area Detector Diffraction System (GADDS). Average grain sizes within the nanoparticle samples were determined from the XRD spectra using the Scherrer equation. The correction for instrumental broadening was conducted using the standard Al_2O_3 sample.

Atomic Force Microscopy: AFM imaging was conducted with an Asylum MFP-3D. Imaging was done in tapping mode with an Olympus AC1160TS probe and at a scan rate of 1 Hz.

Device Fabrication: Silicon-based devices were fabricated from p-doped silicon wafers (resistivity <0.005 W-cm ,with ~300 nm thick thermal oxide) purchased from Addison Engineering Inc. Metal layers for all devices (with the exception of the MSIM capacitors) were deposited using lift-off techniques. For the MSIM capacitors, a shadow mask was utilized to deposit the gold films onto the nanoparticles. Electron-beam evaporation was used throughout for metal deposition.

FET Measurements: All FET measurements were taken with a Karl Suss PM6 probe station equipped with Keithley 237 source measurement units.

Capacitance-Voltage Measurements: C-V data were taken with an Agilent 4284 Precision LCR meter equipped with an Agilent 16047A Text Fixture. The H_{pot} and H_{cur} leads are connected to the gate (doped-Si), and the L_{pot} and L_{cur} leads are connected to the reference (Au).

X-ray Photoelectron Spectroscopy (XPS): XPS data were collected on a Surface Science Instruments SSX-100 operating a pressure < 2×10^{-9} Torr and with monochromatic Al Kα X-rays at 1486.6 eV.

Supplementary Information on Characterization of Nanoparticles and Nanoparticle Films

Scanning electron micrographs and AFM images of films prepared by EPD and spin-casting suggests that EPD films are more compacted. **Figure S1a-d** shows scanning electron micrographs (SEM) of typical $Cu_{2-x}S$ films deposited by EPD and spin-casting, treated with ammonium sulfide, that was measured in our studies. The SEM images were processed with ImageJ software (National Institute of Health) in order to assess the packing of the film. By first applying high contrast to the SEM images and thresholding the resulting image, the pores and particles in the image are counted and sized. [2] Upon analyzing images of the EPD and spin cast films in **Figure S1b** and **d**, the percentage area of the nanoparticles is found to be 63% and 40%, respectively, suggesting that the EPD films are more compacted than spin-cast films for all the films observed in the SEM. This basic particle count analysis, which focuses mostly on the topmost layer of the films, could be improved by carrying more rigorous pore sorption measurements in the future. Tapping mode height and phase AFM images of EPD and spin cast films are taken to further understand the film compaction as shown in **Figure S1e-h**. The root mean square (rms) roughness of the 1 μm x 1 μm scan area of the EPD and spin-cast film is 6 nm and 14 nm, respectively. (We note that the AFM images were taken using a tip of radius of ~8 nm; hence, the images do not laterally resolve individual particles ~5 nm in diameter.) The phase images (**Figure S1g** and **h**), which monitor the phase lag between the drive signal of the cantilever and the actual cantilever oscillation, reveal the homogeneity of the deposited films of the films as tip interaction with different materials result in different phase offsets. In addition, the phase images show that the porous region of the films have a larger phase offset than regions with nanoparticles, providing better visualization of the packing of the films. These

results suggest that EPD forms more closely packed nanoparticle films than spin-cast films and are thus likely to have better interparticle coupling, corroborating the observation from the SEM images.

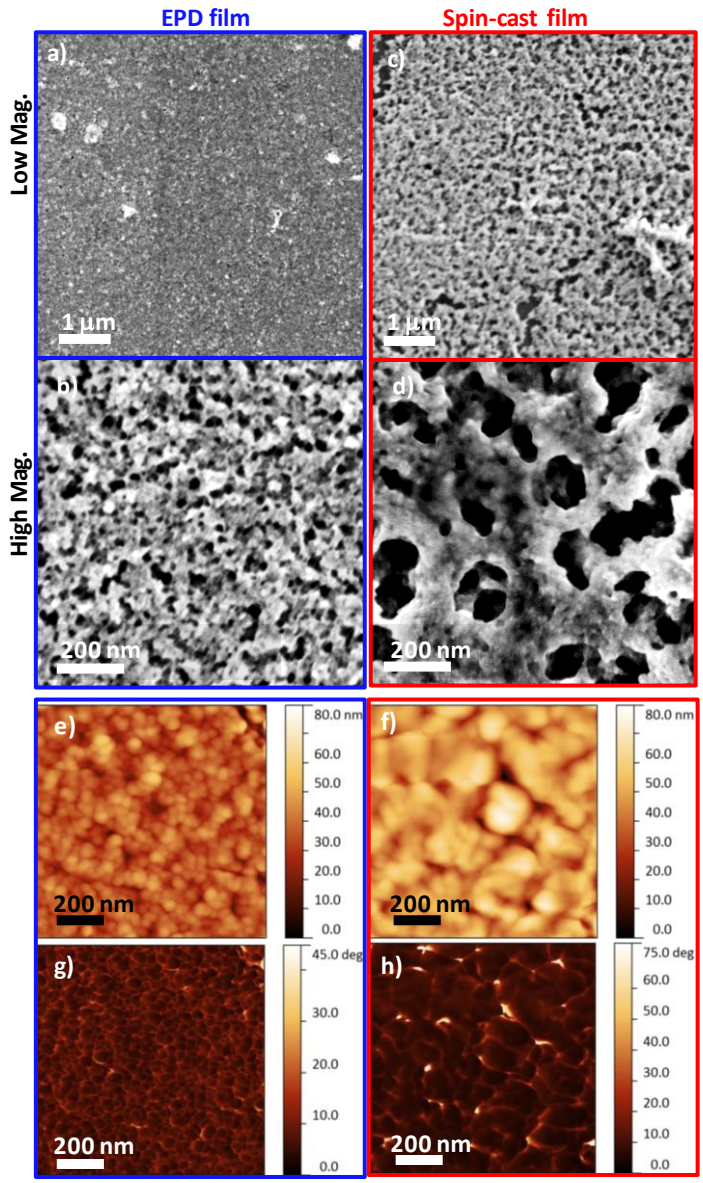

Figure S1. SEM and AFM images of EPD (blue outlines) and spin-cast (red outlines) films treated with ammonium sulfide. a-d) Low and high magnification SEM micrographs of typical EPD (a,b) and spin-cast

films (c,d) after ammonium sulfide treatment. EPD is shown to form more tightly packed films than spin-cast films. e) AFM height image of typical EPD film. f) AFM height image of typical spin-cast film. g) AFM phase image of typical EPD film. h) AFM phase image of typical spin-cast film.

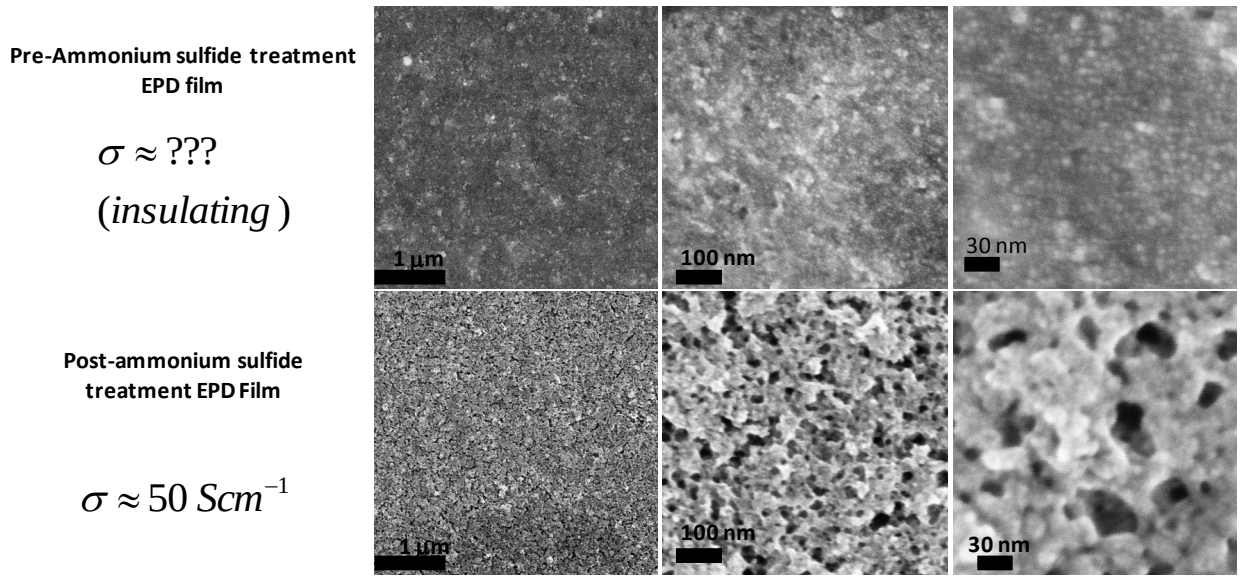

Figure S2. SEM of EPD films with and without ammonium sulfide treatment. Magnification increases from left to right. Without the ammonium sulfide treatment that links the particle together, the EPD films are insulating.

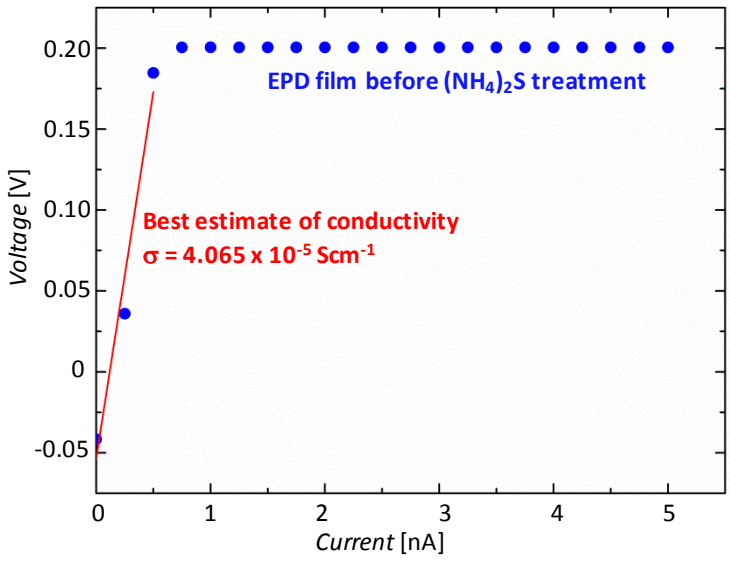

Figure S3. Four-wire resistance measurement of EPD pre-ammonium sulfide treatment. Measurement instrument (Keithley 237) reaches compliance voltage of 0.2 V at 1 nA of source current. This implies that the sheet resistance will be in the order of GΩ; hence, we can conclude the films are insulating before ammonium sulfide treatment.

Supplementary discussion: **Percentage Area Estimation with ImageJ**

From the SEM images of the nanoparticle films in Figure S1, we observed that the EPD films appear to have smaller pore sizes then spin-cast films. However, in order to obtain a more quantitative estimate of the percentage area of the images that consist of nanoparticles, the SEM images were processed with ImageJ. We note that since the films are made from multiple deposition cycles, this analysis method is mostly providing information about the topmost layer of the films. First we enhance the contrast of the images by 100% to better distinguish the nanoparticle regions and the pores—leading to a binary image with higher pixel intensity for the nanoparticle regions, and low intensity for the pore regions, since the original SEM images are grayscale. With ImageJ, we

made sure a threshold value of 129 is obtained for the enhanced contrast images, which implies converting the original grayscale images into binary images with only two pixel values, 0 and 255, corresponding to pore regions and nanoparticle regions respectively. The percentage of pixels with 255 value then represent the area occupied by the nanoparticles. The results are shown in **Figure S4.**

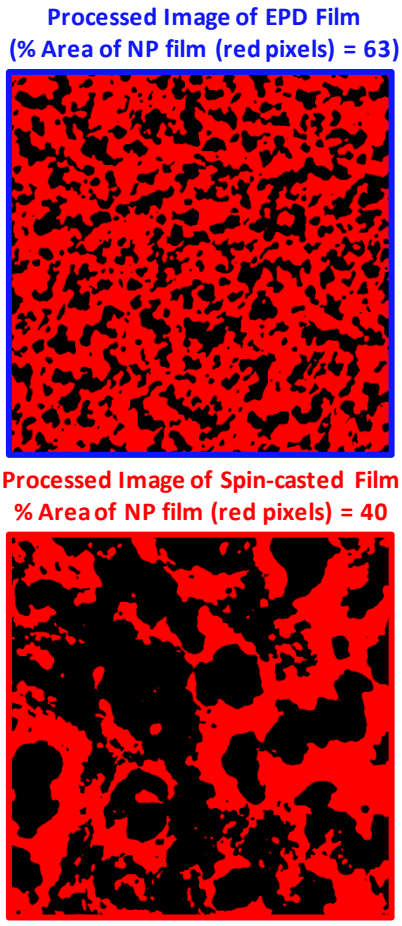

Figure S4. ImageJ-processed images of SEM micrographs of EPD and spin-cast films (Figures S1b and S1d). Images are processed following standard procedures [2]. EPD films has large percentage area of nanoparticles (63%) than spin-cast films (40%) suggesting better film better compaction, which likely enhances interparticle coupling. Since films involve several deposition layers, this type of image analysis is biased to analyze mostly the top layer of the film.

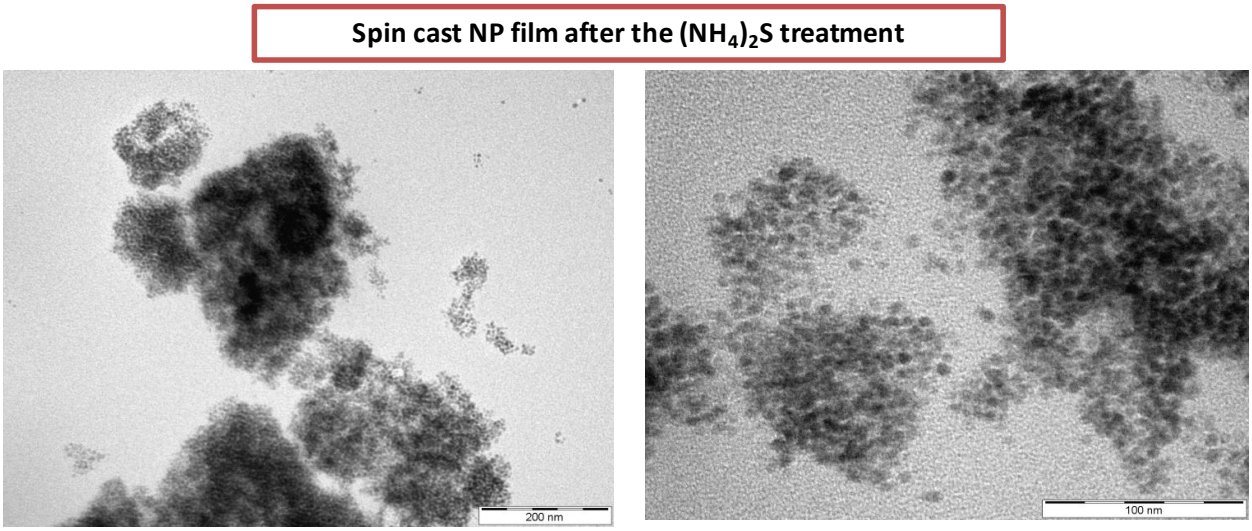

Figure S5: Low and high magnification TEM images of nanoparticles scrapped off from spin-cast films treated with ammonium sulfide. Nanoparticles do not appear to be sintered, but are tightly connected.

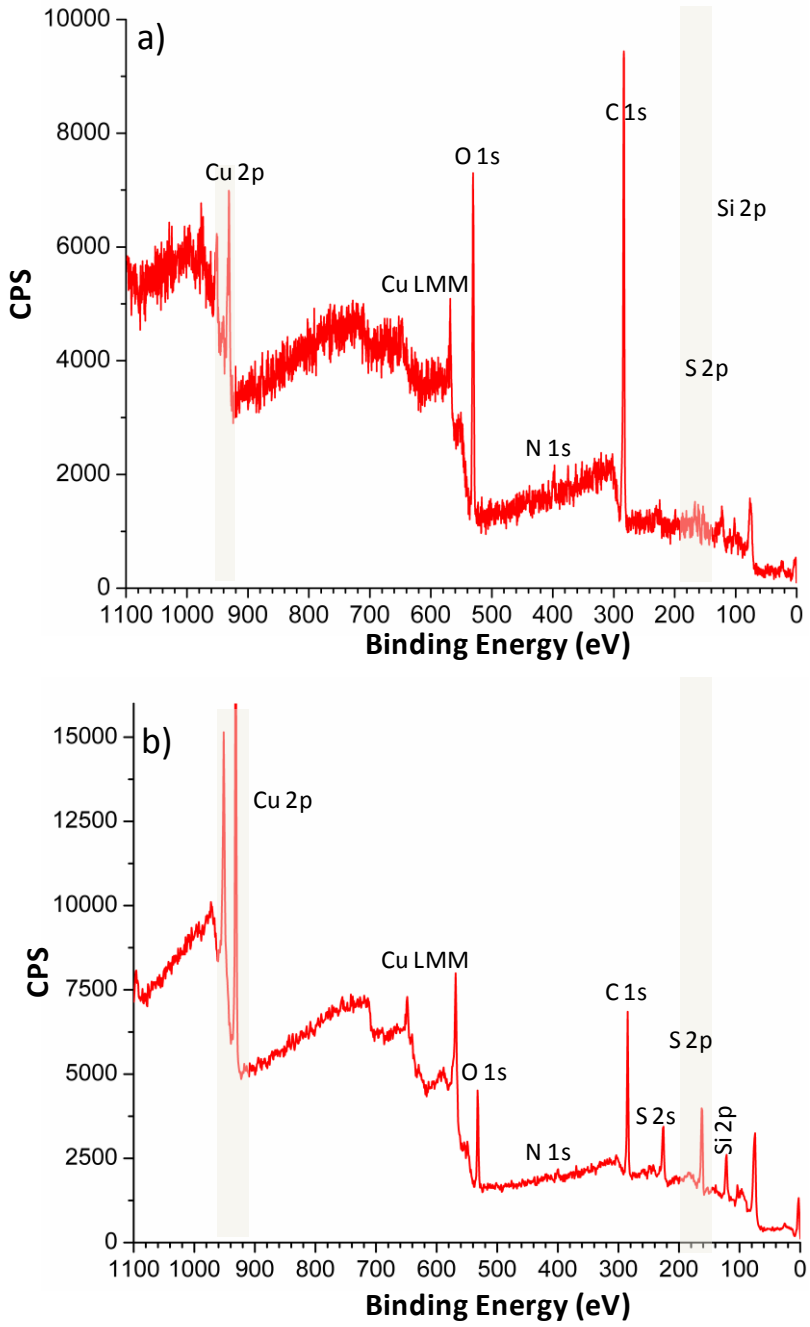

Figure S6. XPS survey scan of spin-cast film. a) pre-ammonium sulfide treatment. b) post-ammonium sulfide treatment.

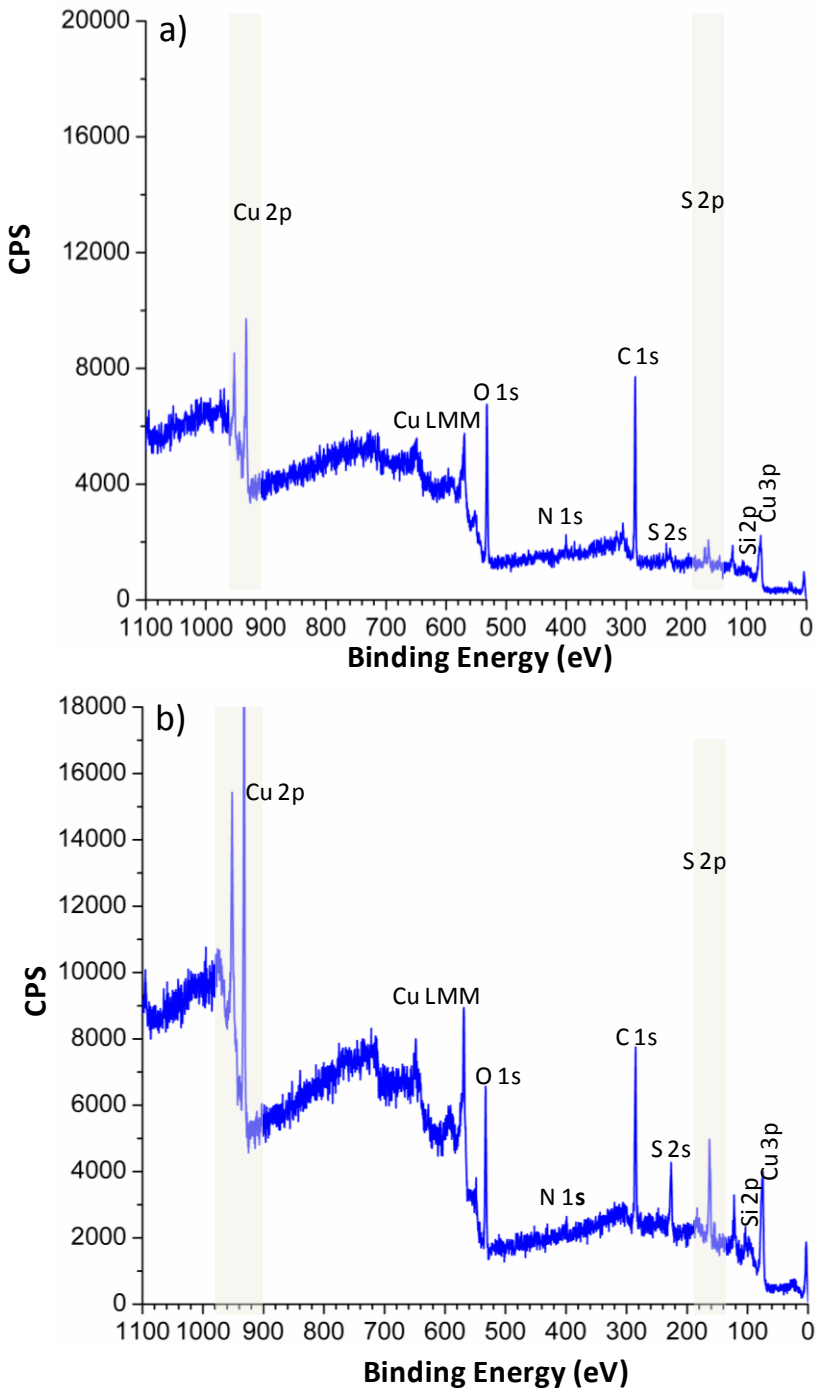

Figure S7. XPS survey scan of EPD film. a) pre-ammonium sulfide. b) post-ammonium sulfide treatment.

Table S1. Summary of atomic percentages of elements analyzed in XPS spectra of spin-cast and EPD films before and after ammonium sulfide treatment. Films for XPS studies were deposited on doped-Si/SiO_2 substrates.

Element	Spin-cast before $(NH_4)_2S$	Spin-cast after $(NH_4)_2S$	EPD before $(NH_4)_2S$	EPD after $(NH_4)_2S$
C	70.49	32.48	65.07	49.4
O	21.08	17.25	24.02	14.64
N	2.15	2.87	2.1	0.45
Cu	**4.12**	**22.03**	**5.96**	**14.72**
S	**1.99**	**22.19**	**2.81**	**17.55**
Si	0.16	2.78	0	3.24

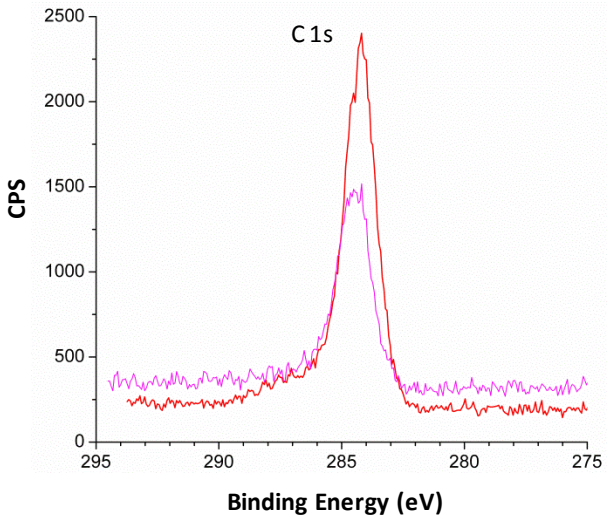

Figure S8. High resolution XPS scan of the C 1s region for spin-cast before (red) and after (magenta) ammonium sulfide treatment.

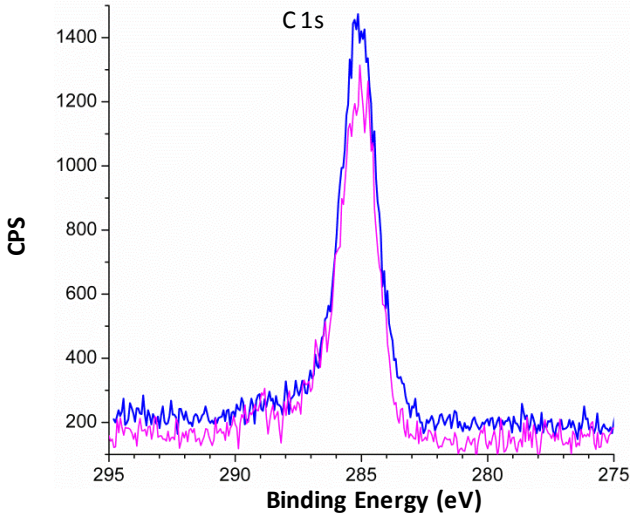

Figure S9. High resolution XPS scan of the C 1s region for EPD film before (blue) and after (magenta) ammonium sulfide treatment.

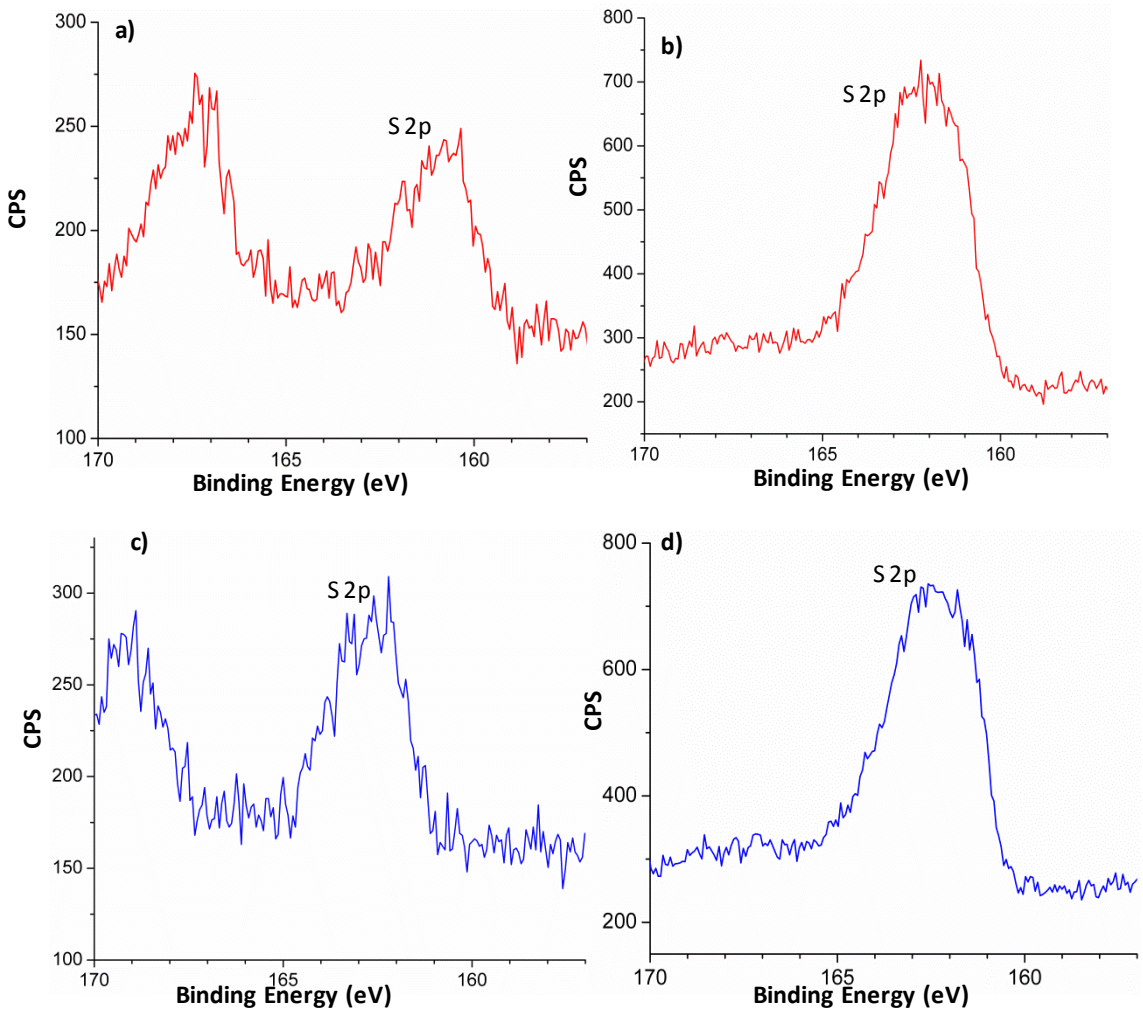

Figure S10. High resolution XPS scan of the S 2p region for spin cast films (a) Spin-cast film before ammonium sulfide treatment. (b) Spin-cast film after ammonium sulfide treatment. (c) EPD films before ammonium sulfide treatment. (d) EPD films after ammonium sulfide treatment.

Table S2. Comparison of our nanoparticle-based $Cu_{2-x}S$ films to previous work.

Synthesis	Deposition method	Stoichiometry (x in Cu_xS)	Stoichiometry determination	Film thickness	Conductivity [Scm^{-1}]	Reference
Copper target in Ar-H_2S-H_2 atmosphere/ Cu1.8S source	RF sputtering/ Evaporation	1.995 and 1.999	Electrochemical methods	0.1-0.5 μm / 1 μm	35 and 7	Wagner et al. [3]
Copper in H_2S/Ar atmosphere	RF sputtering	Not specified	None	1 μm	17.6	Leong et al. [4]
K15 (based on Cu(hfac)(tmvs))	Pulsed CVD	1.9-2.0	EXAFS	120 nm	18.5	Carbone et al. [5]
Aqueous Cu thiosulfate	Chemically deposited	1.8 and 2.0	Rutherford backscattering analysis, and film color	120 nm and 80 nm	277 and 69	Grozdanov et al.[6]
Bath of Coper chloride, triethanolamine, ammonia, sodium hydroxide, thiourea, and DI water	Chemically deposited	1.8	X-ray diffraction	100 nm	2000-10000 (after annealing)	Cardoso et al. [7]
Bath of Coper chloride, triethanolamine, ammonia, sodium hydroxide, thiourea, and DI water	Chemical bath deposition	Not specified	Comparison with reported stoichiometry-dependent sheet resistance	150 – 350 nm	1 -250 (annealed and dependent on deposition time)	Nair et al. [8]
Dissolution of copper chloride in a mixed solution of water ammnonium hydroxide, TEA, and thiourea	Surface induced nucleation and in-situ assembly	1.75	Electron diffraction	~100 nm	~2000	Liufu et al. [9]
Heat-up colloidal synthesis (Copper chloride and oleylamine) [1]	Spin-casting + ammonium sulfide treatment / EPD + ammonium sulfide treatment	1.94-1.96	X-ray Diffraction	~120 nm	5.7 / ~75	This work

Table S3. Determination of percentage porosity in EPD and spin-cast films.

Deposition Method	Mass (mg)	Height (nm)	Volume (cm^3)	Density (g/cm^3)	Porosity %	Solid Fraction
Spin	0.08	149	3.35×10^{-5}	2.39	57	0.43
EPD	0.12	154	3.47×10^{-5}	3.46	38	0.62

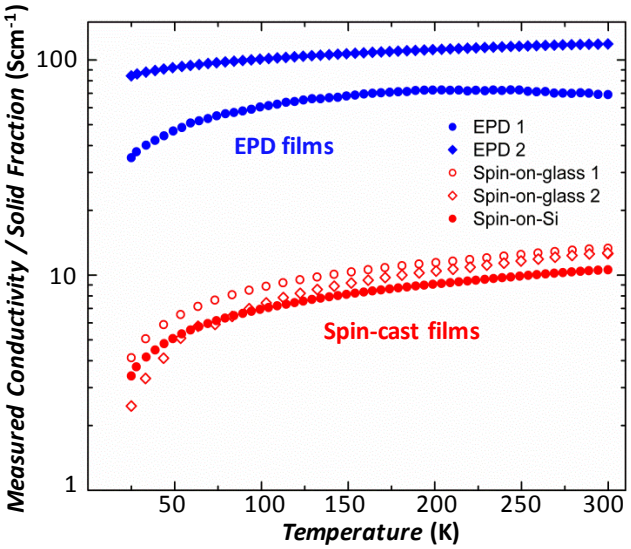

Figure S11. Temperature-dependent conductivity normalized by the solid fraction of copper sulfide to express the interlinking nanoparticle conductivities of EPD and spin-cast films. EPD and spin-cast films have ~38% and 57% porosity, respectively. By rescaling the conductivity plot in Figure 5a of main text, we show that the lower porosity in EPD films alone does not account for the increase in conductivity

Table S4. Adjusted-R^2 of linear fits of the temperature-dependence of conductivity to nearest-neighbor hopping, Efros-Shklovskii variable-range hopping, and Mott variable-range hopping.

Sample	Adjusted $-R^2$ values of linear fits of conductivity with different powers of temperature (T)		
	$1/T$	$1/T^{0.5}$	$1/T^{0.25}$
EPD1	0.962	0.970	0.950
EPD2	0.852	0.951	0.982
Spin-on-Si	0.928	0.989	0.999
Spin-on-glass 1	0.936	0.993	0.999
Spin-on-glass 2	0.949	0.996	0.996

.

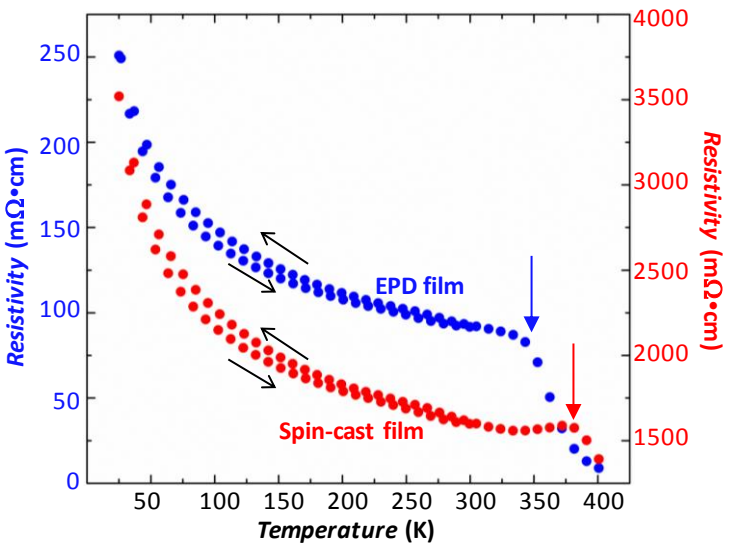

Figure S12. Plot of temperature-dependent resistivity of EPD and spin-cast films that have been thermally cycled from 300 K to 25 K, and then from 25 K to 400 K. 400 K is the maximum temperature obtainable in our measurement apparatus (PPMS). The blue and red arrows indicate the onset of a sharp drop in resistivity for EPD and spin-cast films, respectively. This irreversible increase in conductivity is possibly due to sintering of the nanoparticles in the films or thermal doping. The films measured in this plot have poorer performance than samples from the main text due to aging.

Supplementary Discussion: Film performance over time

The conductivity of one of the spin-cast films measured in ambient over time suggest a degradation in film performance with time as shown in **Figure S13**: After ~50 days, room temperature conductivity remains the same order of magnitude, but after ~140 days, room temperature conductivity drops by and order of magnitude. Such studies will be important considerations needed for practical applications. Perhaps, the films should not be stored in ambient conditions for a lengthy study.

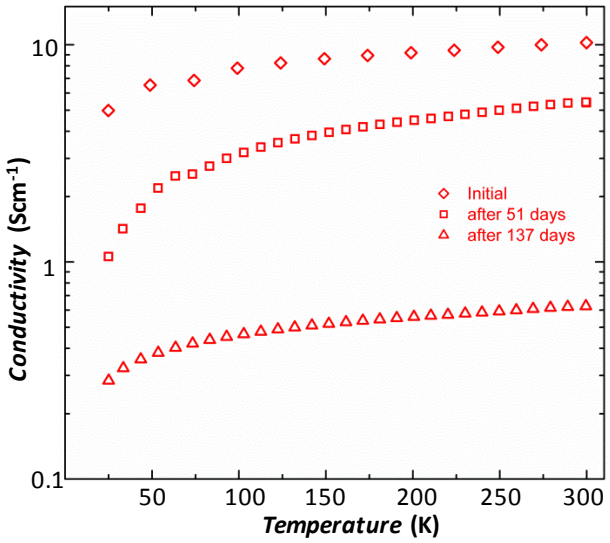

Figure S13. Plots of conductivity of a spin-cast film over time. After ~50 days in ambient condition, the spin-cast film has about the same order of magnitude room-temperature conductivity, but drops about ½ in value. Film conductivity degrades over time when left in ambient conditions.

Supplementary Discussion: Light Stability

In order to assess the sensitivity of the films to light, four-wire resistance measurements of the films deposited on two gold electrodes of varying spacing (50 to 400 μm) were performed in dark (in an enclosed probe station) and in light (with Microlite FL2000 150 W Fiber Optic Illuminator). We observed negligible changes in film resistance in the films as shown in **Figures S14 and S15**. In addition, the resistance of the EPD films increases with increasing electrode spacing suggesting a more uniform film, while the spin-cast films appear to have an inhomogeneous coverage.

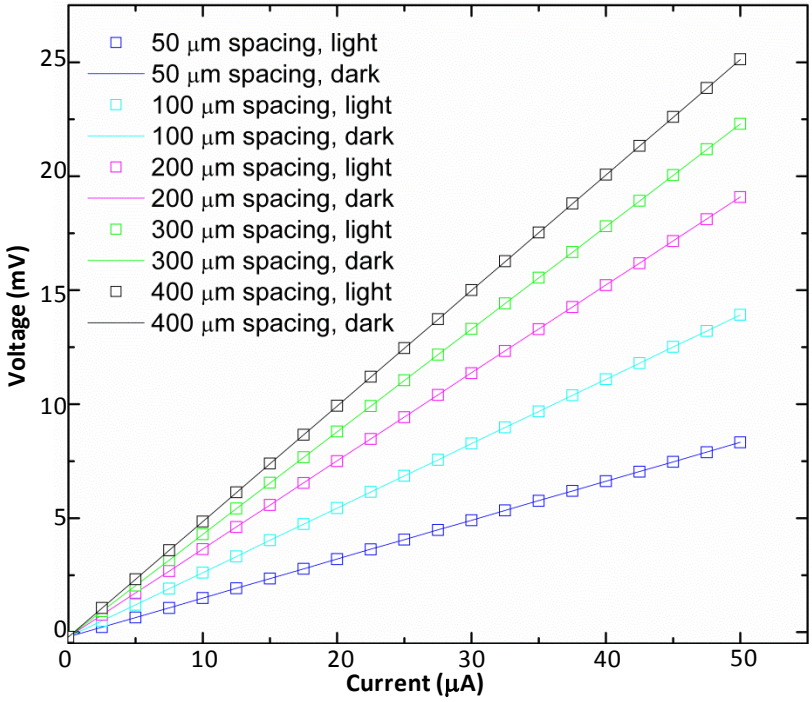

Figure S14. Current-Voltage (I-V) measurements of EPD films in the dark (lines) and under illumination (squares) with a 150 W illuminator showing negligible light sensitivity. 4-wire resistance measurements were performed with films deposited on Au electrodes with varying spacing (50 to 400 μm).

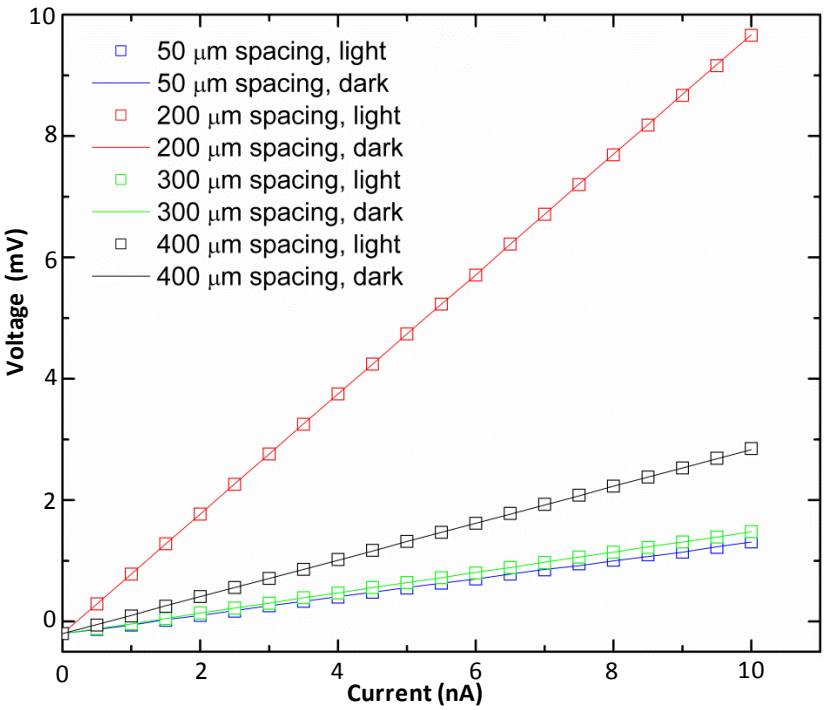

Figure S15. Current-Voltage (I-V) measurements of spin-cast films in the dark (lines) and under illumination (squares) with a 150 W illuminator showing negligible light sensitivity. 4-wire resistance measurements were performed with films deposited on Au electrodes with varying spacing (50 to 400 μm).

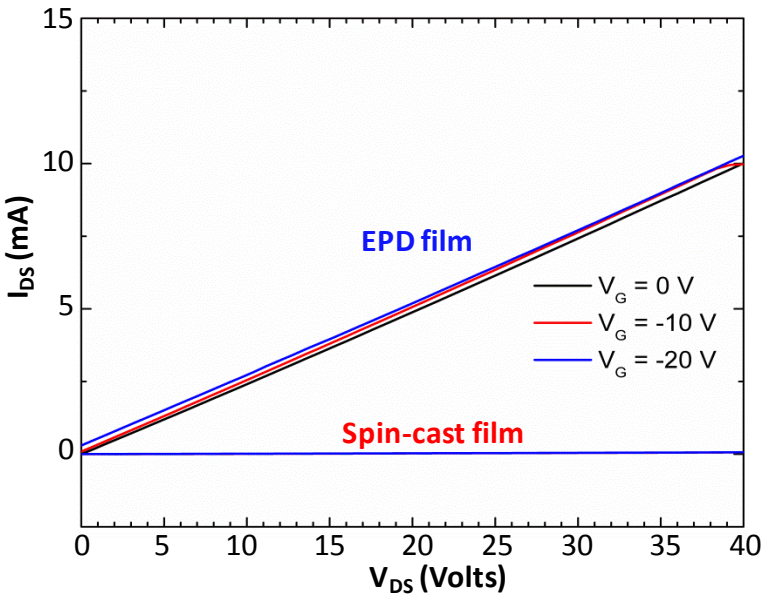

Figure S16. Linear scale plot of drain-source current as a function of drain source voltage (FET output characteristics). Minimal gate modulation is observed. The higher conductivity of the EPD films suppresses the features of the spin-cast film plot when shown in a linear scale. Hence, a log-log plot is shown in Figure 6a.

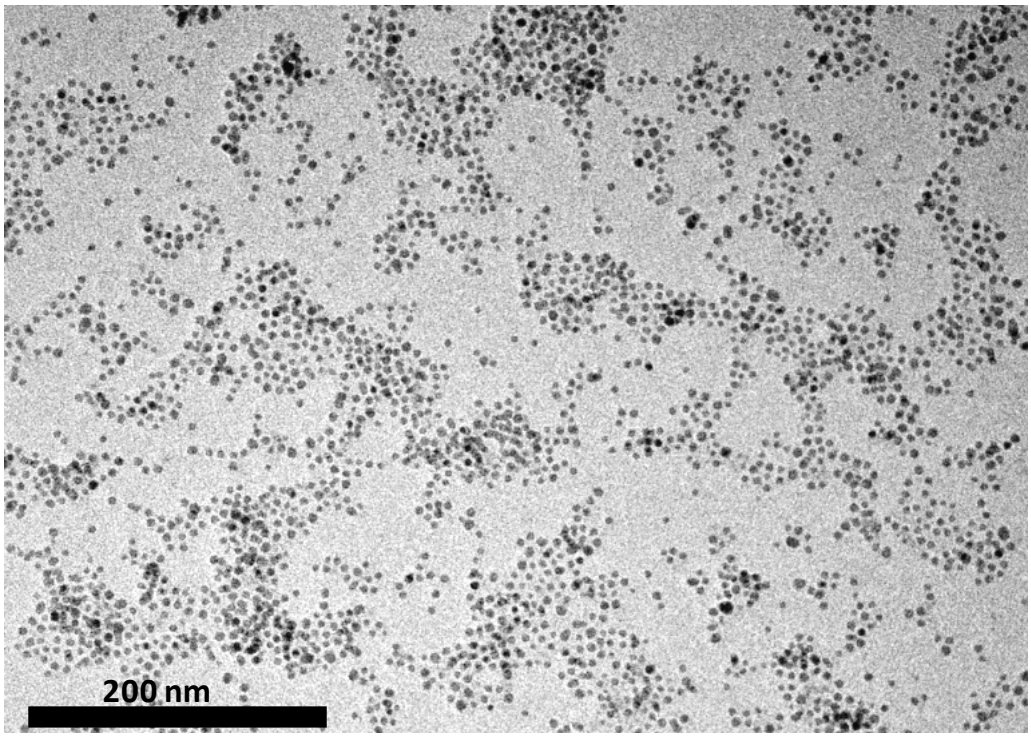

Figure S17: TEM of the starting copper sulfide nanoparticles

References

1. Zhang, H. T.; Hyun, B. R.; Wise, F. W.; Robinson, R. D. A Generic Method for Rational Scalable Synthesis of Monodisperse Metal Sulfide Nanocrystals. *Nano Lett.* **2012,** 12, 5856-5860.
2. Bright, D. S. Digital Image Processing with NIH Image (Mac) and ImageJ *http://www.nist.gov/lispix/imlab/labs.html* **2004**.
3. Wagner, R.; Wiemhöfer, H. D. Hall Effect and Conductivity in Thin Films of Low Temperature Chalcocite Cu2s at 20°C as a Function of Stoichiometry. *J. Phys. C: Solid State Phys.* **1983,** 44, 801-805.
4. Leong, J. Y.; Yee, J. H. Hall Effect in Reactively Sputtered Cu2s. *Appl. Phys. Lett.* **1979,** 35, 601-602.
5. Carbone, I.; Zhou, Q.; Vollbrecht, B.; Yang, L.; Medling, S.; Bezryadina, A.; Bridges, F.; Alers, G. B.; Norman, J. T.; Kinmen, T. Pulsed Chemical Vapor Deposition of Cu2s into a Porous TiO2 Matrix. *J. Vac. Sci. Technol. A* **2011,** 29, 051505
6. Grozdanov, I.; Najdoski, M. Optical and Electrical-Properties of Copper Sulfide Films of Variable Composition. *J. Solid State Chem.* **1995,** 114, 469-475.
7. Cardoso, J.; GomezDaza, O.; Ixtlilco, L.; Nair, M. T. S.; Nair, P. K. Conductive Copper Sulfide Thin Films on Polyimide Foils. *Semicond. Sci. Technol.* **2001,** 16, 123-127.
8. Nair, M. T. S.; Nair, P. K. Chemical Bath Deposition of Cu X S Thin Films and Their Prospective Large Area Applications. *Semicond. Sci. Technol.* **1989,** 4, 191.
9. Liufu, S.-C.; Chen, L.-D.; Yao, Q.; Huang, F.-Q. In Situ Assembly of Cuxs Quantum-Dots into Thin Film: A Highly Conductive P-Type Transparent Film. *J. Phys. Chem. C* **2008,** 112, 12085-12088.